Application of airborne radiometric surveys for large-scale geogenic radon potential classification

Elío, Javier; Crowley, Quentin; Scanlon, Ray; Hodgson, Jim; Long, Stephanie; Cooper, Mark; Gallagher, Vincent

Published in:
Journal of the European Radon Association

DOI (link to publication from Publisher):
10.35815/radon.v1.4358

Publication date:
2020

Document Version
Publisher's PDF, also known as Version of record

JERA

ORIGINAL ARTICLE

Application of airborne radiometric surveys for large-scale geogenic radon potential classification

Javier Elío[1,2]*, Quentin Crowley[1], Ray Scanlon[3], Jim Hodgson[3], Stephanie Long[4], Mark Cooper[5] and Vincent Gallagher[3]

[1]Centre for the Environment, Trinity College, Dublin, Ireland; [2]Department of Planning, Aalborg University Copenhagen, Copenhagen, Denmark; [3]Geological Survey, Dublin, Ireland; [4]Environmental Protection Agency of Ireland, Dublin, Ireland; [5]Geological Survey of Northern Ireland, Belfast, Northern Ireland

Abstract

***Background*:** Indoor radon represents an important health issue to the general population. Therefore, accurate radon risk maps help public authorities to prioritise areas where mitigation actions should be implemented. As the main source of indoor radon is the soil where the building is constructed, maps derived from geogenic factors ([e.g. geogenic radon potential [GRP]) are viewed as valuable tools for radon mapping.
***Objectives*:** A novel indirect method for estimating the GRP at national/regional level is presented and evaluated in this article.
***Design*:** We calculate the radon risk solely based on the radon concentration in the soil and on the subsoil permeability. The soil gas radon concentration was estimated using airborne gamma-ray spectrometry (i.e. equivalent uranium [eU]), assuming a secular equilibrium between eU and radium (^{226}Ra). The subsoil permeability was estimated based on groundwater subsoil permeability and superficial geology (i.e. quaternary geology) by assigning a permeability category to each soil type (i.e. low, moderate or high). Soil gas predictions were compared with *in situ* radon measurements for representative areas, and the resulting GRP map was validated with independent indoor radon data.
***Results*:** There was good agreement between soil gas radon predictions and *in situ* measurements, and the resultant GRP map identifies potential radon risk areas. Our model shows that the probability of having an indoor radon concentration higher than the Irish reference level (200 Bq m^{-3}) increases from c. 6% (5.2% – 7.1%) for an area classified as Low risk, to c. 9.7% (9.1% – 10.5%) for Moderate-Low risk areas, c. 14% (13.4% – 15.3%) for Moderate-High risk areas and c. 26% (24.5% – 28.6%) for High risk areas.
***Conclusions*:** The method proposed here is a potential alternative approach for radon mapping when airborne radiometric data (i.e. eU) are available.

Keywords: *radon mapping; geogenic radon potential; gamma-ray spectrometry; uranium; soil gas*

Globally, radon is the second most common cause of lung cancer in smokers and the primary cause of lung cancer in non-smokers (1–3). Although the adverse health effects of radon exposure are a significant public health issue, these effects may be mitigated if appropriate control measures are implemented (4). In this regard, radon maps are used by regional and national authorities to support policies that protect the general population against the harmful effects of ionising radiation (e.g. 5–7). The main goal of radon maps is to delineate areas where high radon concentrations may be expected, in order to 'prioritize' these areas in a National Radon Action Plan (8, 9). Radon maps may also be used as a basis for determining if preventive measures are required in new buildings, or if radon measurements are required in workplaces (e.g. 10).

The definition of Radon Priority Areas (RPAs) is ambiguous and several criteria (not mutually exclusive) may be applied, depending on political, public health, economic, and other decisions (8, 11). The European Commission (EC), for example, defines RPAs as 'areas where the radon concentration (as an annual average) in a significant number of buildings is expected to exceed the relevant national reference level' (7). However, the EC does not define 'a significant number of buildings' and the reference level is only set as ≤ 300 Bq m^{-3}, with the specific value dependent on individual national policies. Furthermore, the definition of an 'area' is not specified and may be defined by political boundaries (e.g. municipalities and districts) or regular geographical units (e.g. grid cells of 10 × 10 km or 1 × 1 km). Bossew

(8) has discussed the definition and limitations of RPAs in more detail.

Radon maps are normally based on indoor radon measurements, with geogenic factors sometimes used to improve predictions (e.g. 12–18). National maps based only on geological information (i.e. geogenic radon maps) are unusual (19). For example, the geogenic radon potential (GRP) map of Germany only takes into account radon in soil gas and soil permeability (20). This latter approach has the advantage that it measures or estimates the amount of radon that the earth is delivering, and therefore it is assumed that the resulting map is independent of building type (21). The approach that uses both indoor radon measurements and geogenic information, on the other hand, has the advantage of taking account of the radon concentration at the point of exposure (12).

A fundamental problem with radon maps based on indoor radon measurements is that they have legal implications in workplaces and public buildings but they are usually developed using indoor radon measurements made in residential dwellings. Since indoor radon behavior in workplaces and domestic dwellings may not be comparable, due to changes in how buildings are used and constructed (e.g. 22–24), the applicability of indoor radon maps for legislation in workplaces and public buildings may therefore be questionable (8). Maps that do not depend on building characteristics (e.g. GRP maps) would be preferable in this regard.

Estimation of GRP is a common practice in order to assess the risk of having high indoor radon concentrations in new buildings (e.g. in the Czech Republic), with the Neznal formula (25) being one of the most common methods used for this purpose. At a local scale, this approach may be also valid (26) but in many cases it may be impractical to have sufficient *in situ* representative data to develop GRP maps at national and/or regional scales.

Here we test a new approach to develop national/regional GRP maps based on gamma-ray spectrometry radiometric measurements (i.e. eU) and subsoil hydraulic permeability. Such datasets are often collected for geological applications and may thus be available in many countries, but not specifically collected or used for radon mapping. For the analysis in this study, we have used data from the Tellus project, a national mapping programme that is collecting geochemical and geophysical data from Ireland and Northern Ireland (www.gsi.ie/tellus and http://www.bgs.ac.uk/gsni/tellus/overview/). Independent indoor radon measurements and *in situ* soil gas measurements have been used to validate the results. To date, the Tellus airborne geophysical programme has completed coverage of approximately 70% of the island of Ireland, and data are freely available on the Tellus website. The project started in Northern Ireland in 2004–2008, continued into the border region of Ireland (2011–2013), the north midlands region (2014–2015), eastern midlands region (2015), Galway and Waterford areas (2016), Mayo and Donegal (2018), and southeast Ireland (2019). The 2019 data were not available at the time of writing. It is expected that complete coverage of the island of Ireland will be accomplished by 2023.

Soil gas radon concentrations were predicted using 1) the measurement of eU at the surface and 2) soil properties (i.e. porosity, density, and radon emanation factor). The Neznal Radon Potential Index (25) was then estimated and compared with indoor radon measurements. Selected test sites were further studied using *in situ* soil gas radon measurements in order to further validate the radon estimations and to assess the applicability of the methodology proposed in this study.

Material and methods

Geogenic radon potential

We use the Neznal formula (25) for estimating the GRP. It bases the radon risk assessment on two main geogenic factors, namely 1) soil gas radon concentration which is the main indoor radon source and 2) soil permeability which is related to the radon transport in the environment:

$$GRP = \frac{C_{Rn}}{(-\log_{10}(k) - 10)} \qquad \text{(Equation 1)}$$

The equilibrium radon concentration in soil gas (C_{Rn} in kBq m^{-3}) and the soil permeability (k in m^2) were assigned values according to the categorization of each parameter, as proposed by Elio et al. (26) and summarized in Table 1.

C_{Rn} and k were averaged by grids of 1 × 1 km and thus the GRP represents an average risk of having high indoor radon levels at the same 1 km^2 unit. The grid cells were classified as 1) Low risk (GRP < 10), 2) Moderate–Low risk (10 ≤ GRP < 22.5), 3) Moderate–High risk (22.5 ≤ GRP < 30), and 4) High risk (GRP ≥ 30) (Table 2).

Table 1. Assigned values for the GRP estimation

Classification	Measured	Assigned
Soil gas radon concentration (kBq m^{-3})		
Extremely high	≥100	110
Very high	70 ≤ Rn < 100	85
High	50 ≤ Rn < 70	65
Moderate	30 ≤ Rn < 50	50
Low	10 ≤ Rn < 30	25
Very low	< 10	5
Soil permeability (−log$_{10}$[k])		
High	< 11	11
Moderate	11–13	12
Low	> 13	13

GRP: geogenic radon potential.

Citation: Journal of the European Radon Association 2020, 1: 4358 http://dx.doi.org/10.35815/radon.v1.4358

Table 2. Geogenic radon potential classification (after 26)

		GRP					
Permeability	**Low**	2	8	17	22	28	37
	Moderate	3	13	25	33	43	55
	High	5	25	50	65	85	110
		Very low	**Low**	**Moderate**	**High**	**Very high**	**Extremely high**
		Radon soil gas classification					

Color scale: blue, Low risk; green, Moderate–Low; yellow, Moderate–High; red, High. *GRP: geogenic radon potential.*

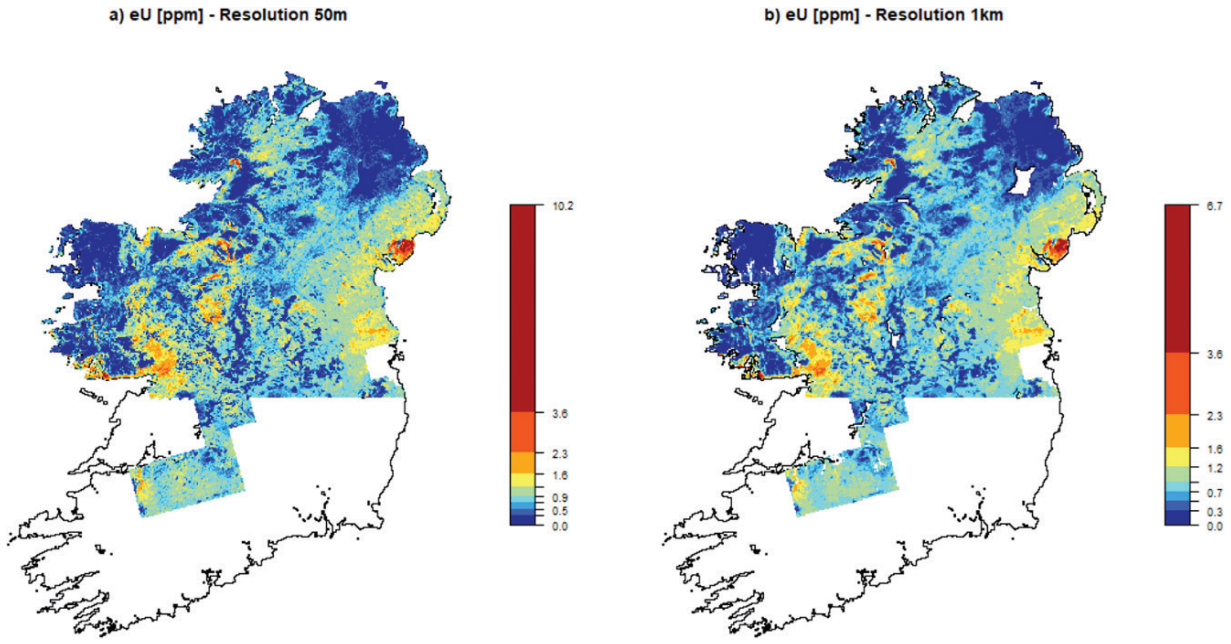

Fig. 1. Equivalent uranium concentration in ppm for a) the initial data at a resolution of 50 × 50 m (breaks: 0.0, 0.3, 0.5, 0.7, 0.9, 1.2, 1.6, 2.3, 3.6, 10.2) and b) the aggregated map at grid cells of 1 × 1 km (breaks: 0.0, 0.3, 0.5, 0.7, 0.9, 1.2, 1.6, 2.3, 3.6, 6.7).

Airborne radiometric survey

The Tellus airborne geophysical survey employs a low-flying aircraft (flying at 60 m in rural areas and 240 m in urban areas) to collect geophysical information on the properties of soils, rocks, and waters. A gamma-ray spectrometer (Exploranium GR820 and Radiation Solution RS-501 from 2018 onward) was employed to measure the concentration of eU (ppm), eTh (ppm), and K (%). The concentrations of uranium (U) and thorium (Th) are expressed as equivalent concentrations since the gamma radiation energy windows used to quantify these elements actually measure ^{214}Bi and ^{208}Tl, respectively, and secular equilibrium in each decay series is assumed (27). All surveys have been merged and the results are available on the Tellus website (www.gsi.ie/tellus). The initial resolution of the data is 50 × 50 m (Fig. 1a), and for the purpose of this study, we aggregated the data into 1 × 1 km grid cells (Fig. 1b), calculating the arithmetic mean (AM) and the standard deviation of eU for each.

Soil gas radon predictions based on equivalent uranium

Radon is a radioactive gas that forms as a decay product of U and Th. However, due to the different half-lives of the isotopes, the radon risk in indoor air is principally caused by ^{222}Rn (28), which is a decay product of ^{226}Ra generated in the radioactive decay series of ^{238}U. ^{222}Rn is generated in the soil matrix due to the presence of ^{226}Ra. It has to be recoiled into the pore space (29), and thus its concentration in soil gas depends both on ^{226}Ra concentration and soil properties, principally soil density, effective porosity, and an emanation coefficient. Therefore, the theoretical ^{222}Rn concentration in soil gas due to ^{226}Ra can be estimated by the following equation (e.g. 30–33):

$$C_{Rn} = \frac{C_{Ra} \cdot \varepsilon \cdot \rho}{n} \cdot \frac{1}{1 - S_F + S_F \cdot K_{W/air}} \qquad \text{(Equation 2)}$$

where C_{Rn} is the ^{222}Rn concentration in soil gas (kBq m^{-3}), C_{Ra} is the ^{226}Ra concentration (Bq kg^{-1}), ε is the

emanation factor (adimensional), ρ is the soil density (g m^{-3}), and n is the effective porosity (adimensional). Water saturation in the pore space ($0 \leq S_F \leq 1$) increases the radon concentration in soil gas (31) since radon is concentrated in the air rather than in the water content of the pore space due to its higher affinity to air than water (i.e. $K_{W/air} = 0.25$, where $K_{W/air}$ is the radon partitioning coefficient between water and air).

Tellus airborne gamma-ray spectrometry radiometric data (i.e. eU in ppm) were aggregated by grid cells of 1 × 1 km. Mean values of radium ($e^{226}Ra$; Bq kg^{-1}) were then estimated assuming secular equilibrium (i.e. ^{226}Ra activity equal to ^{238}U activity), using a conversion factor of 12.35 to transform the eU concentration in ppm to ^{238}U activity in Bq kg^{-1} (34). Although a disequilibrium between ^{214}Bi and ^{238}U is frequent in the natural environment (i.e. equilibrium occurs after more than 1.2×10^6 years), in a closed system, equilibrium between ^{214}Bi and ^{226}Ra occurs after approximately 30 days and thus airborne gamma radiometric signals may be related more to the radium activity (^{226}Ra) in soil than to the uranium activity. We maintain, however, the nomenclature of equivalent (eRa) to clarify that we have inferred the concentration using eU.

^{222}Rn concentration in soil gas was then estimated in each 1 × 1 km grid cell using Equation 2. The radon variability in each grid was assessed by Monte Carlo simulations (n = 1,000), assuming that 1) ε, ρ, and n are normally distributed with typical values of 0.29, 1.35 g m^{-3}, and 0.30 and standard deviations of 0.03, 0.06, and 0.07, respectively (35), and 2) a uniform distribution of water saturation coefficient (S_F) with a minimum of 0.4 and a maximum of 0.6 (Fig. 2). The 75th percentile of simulated soil gas radon concentrations in each grid cell was then used for the GRP calculation (i.e. C_{Rn} measured in Table 1). The selection of the 75th percentile (P75) is arbitrary, and other values could be chosen (e.g. P50 and P95). However, changing the percentile cut-off will affect the outcome (GRP). Lower values (e.g. P50) would reduce the size of areas classified as high risk, and vice versa. We therefore consider that P75 is a reasonable value for not being under/over-protective.

Subsoil permeability

Subsoil permeability has been classified into three categories: 1) Low, 2) Moderate, and 3) High, based on the Groundwater Subsoil Permeability (GWSP) map of Ireland (36) and the all-Ireland Quaternary map (37, 38) (Fig. 3). The GWSP divided the country in three categories, depending on how easily water can infiltrate subsoils, that is 'High', 'Moderate', or 'Low'. We have therefore assigned these categories for the model, and where there is no datum (i.e. areas where subsoil is <3 m thick and in Northern Ireland), we inferred it by assigning a soil permeability to each Quaternary deposit type following the classification proposed by Appleton et al. (39, 40). Furthermore, in the areas of the Quaternary map where there is no datum, 'Bedrock' was assigned as the soil type. This was then split into two types of permeability depending on whether the aquifer bedrock is karstified or not, as described in the GSI Groundwater Resources (Aquifers) – Aquifer Bedrock map (36) (Table 3). The resulting-derived all-Ireland soil permeability map can be seen in Fig. 3.

Indoor radon concentrations

Indoor radon measurements were collected by the Environmental Protection Agency (EPA) as part of national surveys (www.radon.ie). Indoor radon was sampled by passive detectors installed in homes for a period of at least 3 months, and the readings were seasonally adjusted to represent an annual average (14). Two different datasets are available for comparing the GRP classification and the risk of having indoor radon concentration higher than the national reference level of 200 Bq m^{-3}. The first data set corresponds to indoor radon

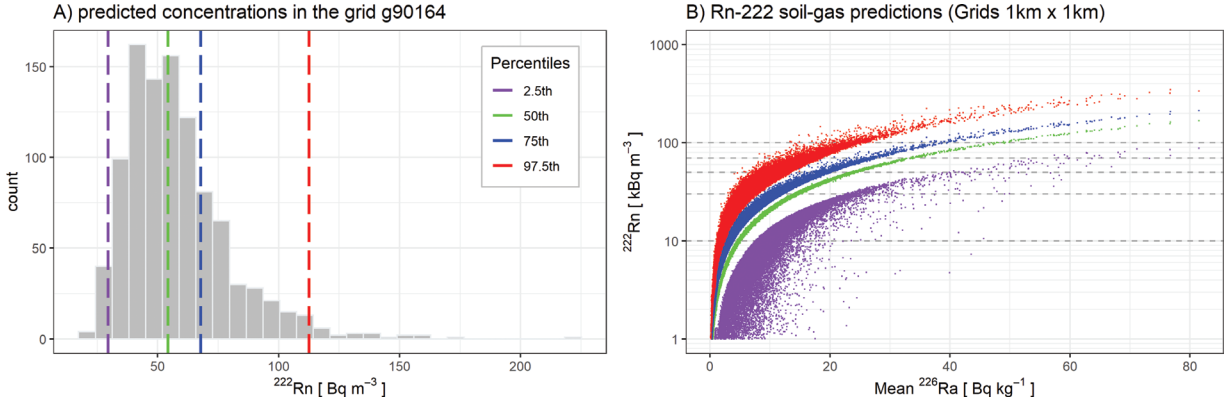

Fig. 2. A) Example of the predicted soil gas radon concentration in the grid G90164 and B) 2.5th, 50th, 75th, and 97.5th percentiles of the simulated values for all grids covered by the Tellus gamma-ray spectrometry airborne radiometrics.

Citation: Journal of the European Radon Association 2020, 1: 4358 http://dx.doi.org/10.35815/radon.v1.4358

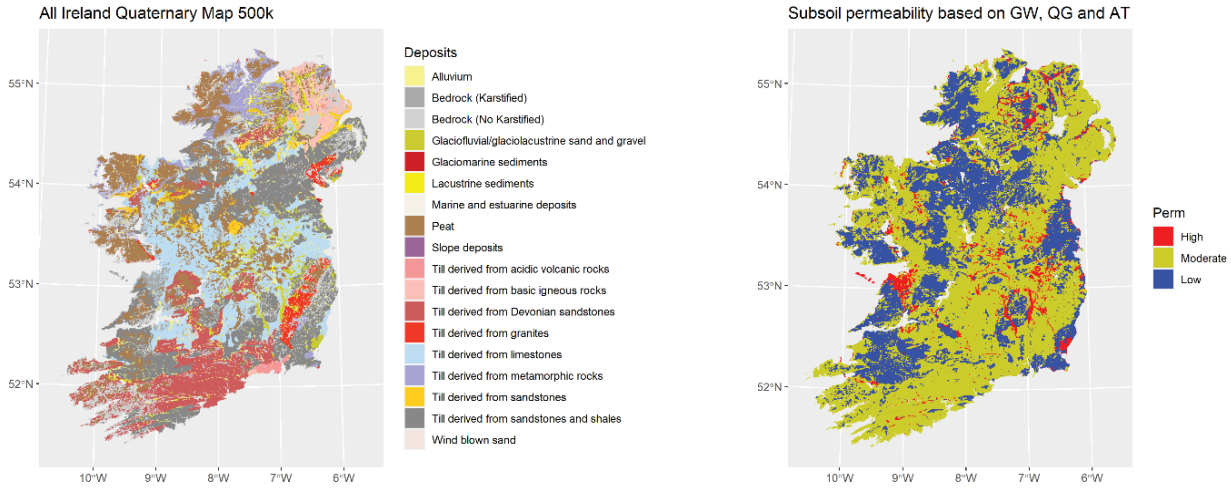

Fig. 3. a) All-Ireland Quaternary geology map (41) and b) derived subsoil permeability map of the island of Groundwater Subsoil Permeability (GW) map of Ireland (36), the all-Ireland Quaternary (QG) map, and the Aquifer Bedrock (AT).

Table 3. Quaternary geology and soil permeability

Description	Soil permeability
Alluvium	Low
Glaciofluvial-glaciolacustrine sand and gravel	High
Glaciomarine sediments	Low
Lacustrine sediments	Low
Marine and estuarine deposits	Low
Peat	Low
Slope deposits	Moderate
Tills (all types)	Moderate
Wind blown sand	High
Bedrock (no karstified)	Moderate
Bedrock (karstified)	High

measurements from 1992 to January 2013 ('old survey') and the other to a group of indoor radon measurements collected from February 2013 to June 2017 ('new survey'). The total numbers of dwellings sampled and georeferenced in each national survey were 31,910 and 6,859, respectively. This corresponds to a total of about 16,700 indoor domestic radon measurements in the area covered by airborne radiometrics (Fig. 4).

Soil gas radon concentration

We have carried out independent soil gas radon concentration measurements in selected areas in Ireland, following the protocol described in Elío et al. (26). These measurements were conducted by first introducing a steel hollow probe in the soil at a typical depth of 75–100 cm, allowing manual sampling of the soil gas with a 150 mL syringe. The soil gas sample was subsequently introduced into an evacuated ionization chamber and after 15 min was measured using an RM-2 detector. The lower detection limit of the instrument is around 3 kBq m^{-3} and the uncertainty of radon measurements is below 20%. Further considerations for measuring soil gas radon concentration may be found in Neznal and Neznal (42). Three separate campaigns took place in the summer and autumn of 2017 (June, July, and September). We took soil gas radon measurements from 13 grids of 1 × 1 km, selected to cover a wide range of radium concentrations in soil (i.e. mean values of ^{226}Ra from 6 to 40 Bq kg^{-1}; Table 5 and Fig. 8). Points in each grid were randomly selected and a total of 133 soil gas samples were taken (Table 5).

Results

Soil gas radon classification based on airborne radiometrics (eU)

Figure 5 shows the soil gas radon estimates based on Tellus airborne radiometrics data (eU). We have divided the region into six radon classes (based on the 75th percentile of the simulated data in Fig. 1 and the radon classification of Table 1). The highest values were found in the Mourne mountains (southeast of Northern Ireland), near Galway (central west part of Ireland), near Roscommon (central part of Ireland), and near Donegal town (northwest Ireland). In the 'Soil gas radon predictions' section, we compare the radon predictions with *in situ* soil gas radon measurements.

Geogenic radon potential map

The predicted radon values in soil gas (Fig. 5) and the soil permeability map (Fig. 3) were used to produce the GRP map of Fig. 6. The map is in general agreement with previous indoor radon maps both in Ireland and in Northern Ireland (12, 14, 43, 44). Thus, for example, we can identify high-risk areas near Galway in the west, in the Mourne mountains in the northeast, parts of county Roscommon, counties Leitrim and Sligo, and south of Dublin in the

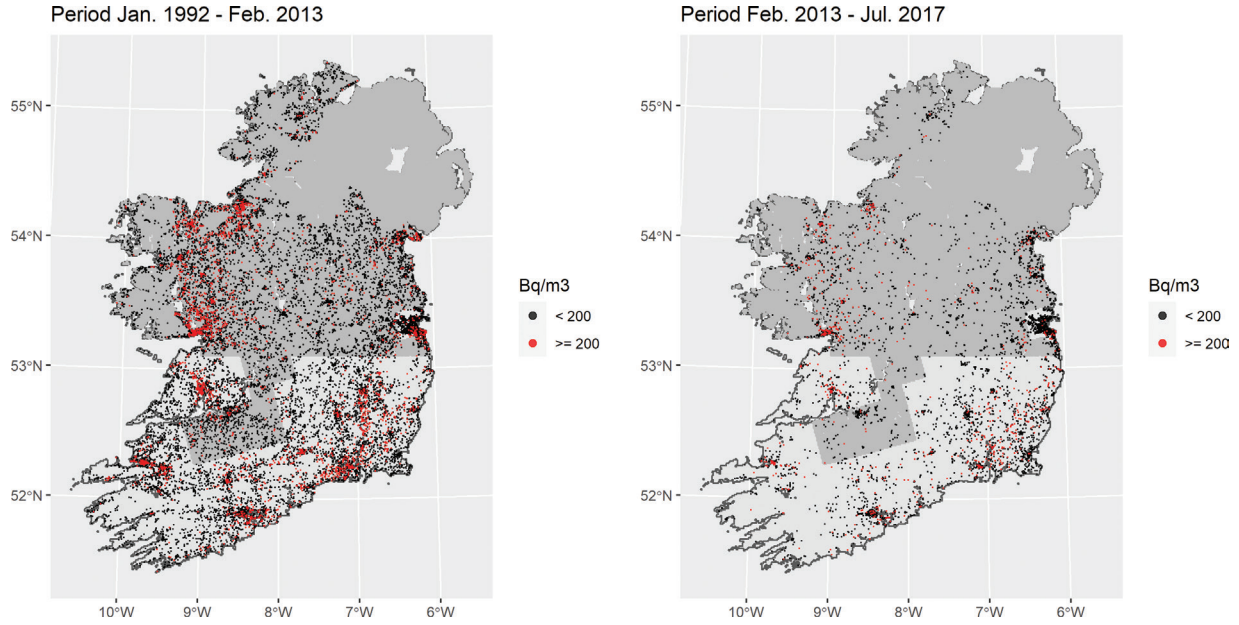

Fig. 4. Indoor radon measurements from the old survey (January 1992–February 2013; $N = 31{,}910$) and the new survey (February 2013–July 2017; $N = 6{,}859$). Dark grey area: part covered by the Tellus airborne survey illustrated in this study. Note that no geolocated indoor radon data are available for Northern Ireland as these are held by Public Health England and were not available for this study.

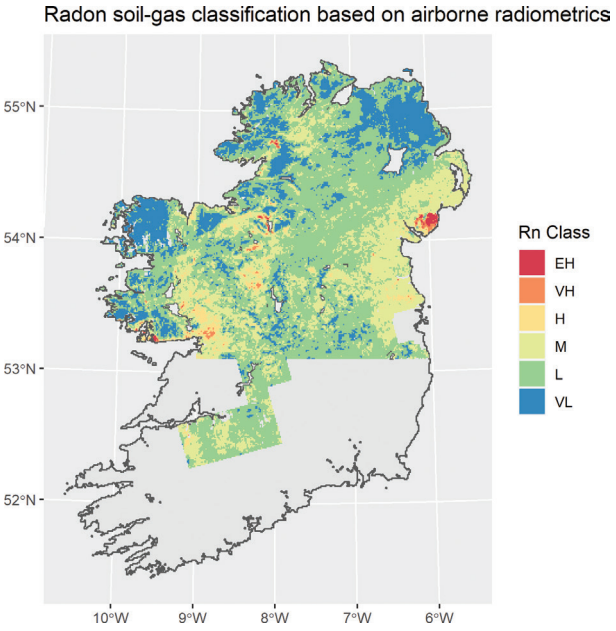

Fig. 5. Radon soil gas classification based on airborne radiometrics.

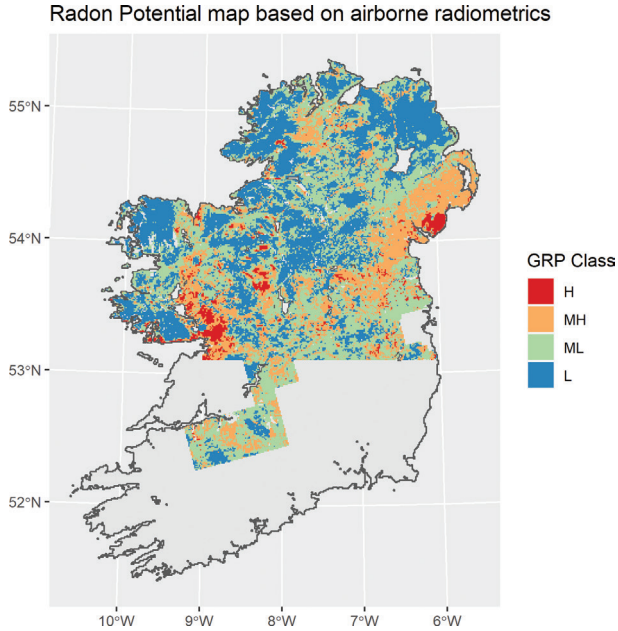

Fig. 6. GRP map based on gamma-ray spectrometry airborne radiometrics and subsoil permeability.

east. Conversely, areas with relatively low risk are also evident and in agreement with previous mapping and modeling (e.g. in the northern part of Northern Ireland and in parts of the west of Ireland). The lack of available geolocated indoor radon for Northern Ireland is not an issue for this map as it does not utilize such measurements.

Indoor radon concentration

Since 1998, Irish building regulations require that new houses built in areas designated as 'high radon areas' (HRA) must have a radon barrier (i.e. areas where the probability of having an indoor radon concentration higher than the national reference level of 200 Bq m^{-3} is

Citation: Journal of the European Radon Association 2020, 1: 4358 http://dx.doi.org/10.35815/radon.v1.4358

10% or higher (45)). The proportion of dwellings with radon prevention measures installed in the new indoor radon dataset, which includes radon measurements from 2013 to 2017, may therefore be higher than in the old one, which includes data from 1992 to 2013. In this regard, the use of indoor radon data from remediated dwellings should be avoided and hence in the new dataset, for any given dwelling, only the first indoor radon measurement was selected, reducing the number of data from 7,007 to 6,859 (second measurements in the same dwelling are assumed to be conducted after remediation activities). However, we were unable to further investigate this source of error since neither dataset contains metadata on building characteristics. Comparison between the old and new indoor radon datasets (Table 4) shows slight differences in summary statistics but the respective histogram and probability plots are almost identical (Fig. 7).

A student-t test indicates that there is no significant difference in the AM of both datasets (P-value = 0.042) but the difference between the mean values of the logarithmic transformed data ($\log_{10}$) is statistically significant (P-value = 0.00014), although very small (i.e. 1.79 for the new dataset and 1.82 for the old dataset). On the other hand, if the indoor radon are treated as a binomial variable with respect to the reference level in Ireland (i.e. 1 when InRn > 200 Bq m^{-3} and 0 otherwise), both datasets have a similar proportion of indoor radon measurements higher than the reference level (Chi-square test; P-value = 0.2082). The probability of having an indoor radon concentration higher than the reference level is 11.9% ($CI_{95\%}$: 11.14–12.69%) and 12.5% ($CI_{95\%}$: 12.10–12.82%) for the new and old datasets, respectively. The spatial distribution of the high indoor radon values in both surveys also seems similar (Fig. 4). It is therefore reasonable to merge both datasets to be used for validating the GRP map.

In situ soil gas radon measurements

The results of *in situ* radon measurements are presented in Table 5. Values range from 13 to 335 kBq m^{-3}. Soil gas radon concentrations vary considerably within individual 1 × 1 km grid cells, with an average relative mean deviation (RMD) of 39% (range 23–55, Table 5). This indicates the difficulty of calculating an average soil gas radon concentration over large areas and also that by doing so we may lose some of the natural spatial variation of the radon soil gas concentrations. The AM and the geometric mean (GM) are also reported in Table 5. Values range from Moderate (i.e. G70565, G70947, and G69054), to High (i.e. G72081 and G56114), Very High (i.e. G98159), or Extremely High (i.e. G78544, G57626, G90163, G78164, G98929, G64863, and G73606) when classified according to Table 1.

Discussion

Soil gas radon classification

Predicted radon measurements, at the 50th percentile level, are lower than the GM of the *in situ* measurements in all cases (Fig. 8), and while in some grids, the predicted values (i.e. 50th percentile) are similar to the *in situ* GM

Table 4. Summary statistics of the new and old indoor radon measurements (Bq m^{-3})

Survey	Dwellings		Min	Q1	Median	AM	Q3	Max	SD	GM	GSD
	Total	InRn > RL									
New	6,859	11.9%	5.0	31.0	55.0	109.7	110.0	6,240	204.47	62.7	2.58
Old	31,910	12.5%	5.7	33.2	59.0	115.3	115.3	9,714	219.72	65.8	2.59

New survey from February 2013 to July 2017; old survey from 1992 to February 2013. *Q1: percentile 25%; AM: arithmetic mean; Q3: percentile 75%; SD: standard deviation; GM: geometric mean; GSD: geometric standard deviation.*

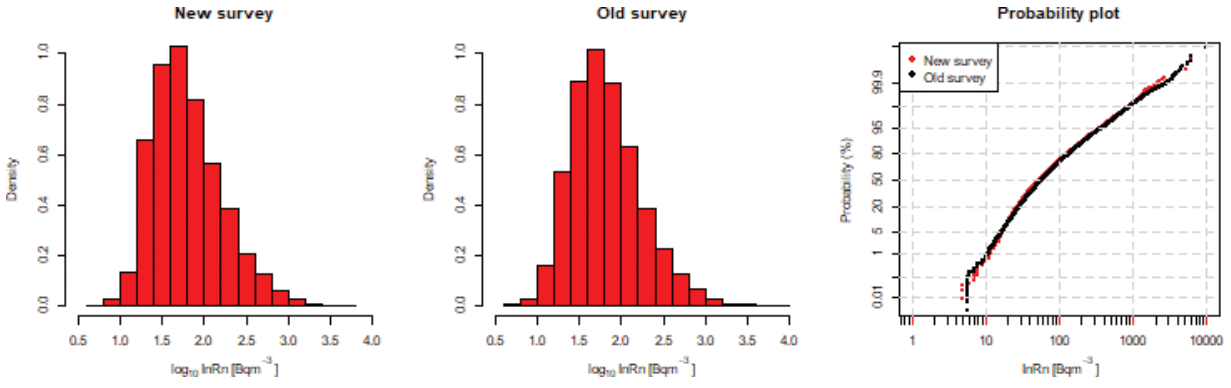

Fig. 7. Histogram and probability plots of the new and old indoor radon measurements.

Table 5. Summary results by grids of 1 × 1 km

Grid	N data	^{222}Rn in soil gas						Estimations based on eU			
		Min	GM	AM	Max	RMD	eRa	eRn			
								P2.5%	P50%	P75%	P97.5%
G56114	9	16	67	80	125	43	6	0	12	17	30
G57626	10	49	108	113	170	23	14	17	29	35	58
G64863	11	85	145	155	310	30	19	23	39	48	77
G69054	9	20	37	40	69	33	14	18	29	35	52
G70565	9	13	33	37	65	38	9	12	19	23	38
G70947	9	13	36	39	59	32	13	16	27	33	54
G72081	9	17	51	60	114	46	12	15	24	30	50
G73606	8	76	179	196	264	33	27	30	55	69	111
G78164	10	79	122	128	191	29	19	23	39	48	76
G78544	10	42	102	120	256	50	23	29	47	58	89
G90163	9	31	111	138	335	51	40	50	84	103	164
G98159	10	16	94	121	260	55	30	37	63	79	129
G98929	10	60	142	163	280	43	36	45	77	93	153

AM: arithmetic mean; GM: geometric mean; RMD: relative mean deviation (%); ^{222}Rn in kBq m^{-3}; eRa: estimated ^{226}Ra concentration in Bq kg^{-1}; eRn: predicted ^{222}Rn concentration in kBq m^{-3}.

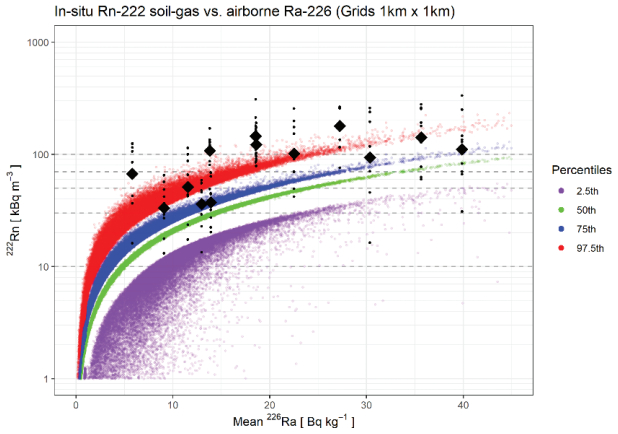

Fig. 8. In situ versus airborne radium (eRa) concentration in soil (color points represent the 2.5th, 50th, 75th, and 97.5th percentiles obtained in the simulation; the black points are the soil gas radon samples; and the black diamonds are the GM of the radon measurements in each grid).

(i.e. G70947, G69054, G98159, and G90163; Table 5), in other cases the relative difference may be up to 80% (i.e. G56114) (Table 5). We acknowledge, however, that soil gas radon concentrations have a large spatial and temporal variability, even at small scale (42), and thus it is difficult to predict a precise radon concentration. At 1 × 1 km scale, it would be even more complicated as suggested by our *in situ* soil gas radon measurements, with RMD ranging from 23 to 55% (Table 5). For this reason, our goal is not to estimate an exact value but to get an order of magnitude of the soil radon concentration, and then evaluate where we can expect high or low values (Table 1). Finally, detailed surveys could be conducted in selected areas if necessary.

Using our approach, a large number of the *in situ* soil gas radon measurements (black points) are within our predictions (Fig. 8). There are grids where predictions and measurements do not match, and the reason for this is currently unknown. However, our results indicate that predicted radon values based on radiometric data are within the range of *in situ* measurements, and therefore they may be seen as reasonable estimates of the equilibrium soil gas radon concentration used in Equation 1.

Some discrepancies between *in situ* and predicted values may arise because estimates only take into account the ^{222}Rn generated in the soil by the presence of ^{226}Ra (eRa), but not other possible radon sources (e.g. radon from groundwater or deep sources carried by other gases in fracture areas). Furthermore, we do not take into account the influence of water saturation on the emanation factor, which will also affect radon concentration in soil gas (46, 47). Predictions were calculated with the same parameters, and thus we did not make adjustments for different soil types (e.g. use of different values of ε, ρ, and n according to the different Quaternary deposits). Therefore, the initial radon predictions based on airborne radiometrics show the potential of this analysis but it requires modification and improvement before being used to predict radon potential with a higher degree of confidence.

Further analysis of the high variability of radon concentration in soil gas within 1 × 1 km grid cells is also

Citation: Journal of the European Radon Association 2020, 1: 4358 http://dx.doi.org/10.35815/radon.v1.4358

necessary (Fig. 8 and Table 5). In some grids, the range of measured soil gas radon concentrations is relatively low (e.g. grids G70565 and G70947), but in others measured radon concentrations vary by an order of magnitude (e.g. grid G90163). A better understanding of the possible causes such as different Quaternary/Bedrock geology, possible transport of radon in groundwater (e.g. karstified areas), influence of subsoil permeability, or geological faults on radon will help achieve a better interpretation of the airborne radiometric data.

Geogenic radon potential versus indoor radon

The probability of having an indoor radon concentration in excess of the reference level of 200 Bq m^{-3} in each GRP area rises with the risk classification, from 6% for a Low-risk area to 26% for a High-risk area (Table 6). The GM of indoor radon concentration in each GRP area is also increased (i.e. from 47 to 98 Bq m^{-3}; Table 6 and Fig. 9). These results suggest that the methodology described here is useful for defining RPAs, and thus when the Tellus project has completed surveying all of the island of Ireland, an all-Ireland GRP map could be developed.

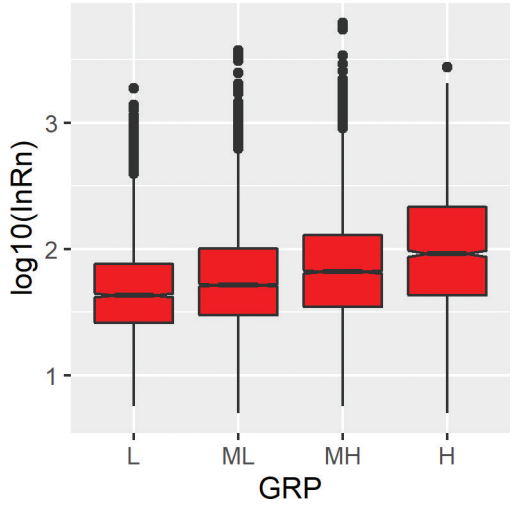

Fig. 9. Boxplot of indoor radon measurements (log_{10}[InRn]) in each GRP (L: Low; ML: Moderate–Low; MH: Moderate–High; H: High).

Conclusion

We demonstrate that the methodology described in this study is useful for radon risk assessment at a national scale. The main advantage of this methodology is that indoor radon measurements are not required and therefore the technique may be applied to rural areas with a low-population density or in areas with no available indoor radon data. Furthermore, since the resulting radon potential map is independent of the type of building and occupancy styles, it may be applied to workplaces, and public and residential buildings.

The risk of misclassification due to sample design, errors in the geocoding of the dwelling addresses, and/or the misunderstanding of building characteristics and living styles is also reduced with our approach. On the other hand, airborne geophysical surveys are expensive and may not necessarily justify a national survey solely for radon protection. However, airborne geophysical surveys are very useful for geological purposes and National Geological Surveys often carry these out to improve knowledge of the national and regional geology (e.g. 48–50), or as a prospecting tool to aid mineral exploration. The approach described here provides an opportunity to add value to existing airborne radiometric datasets.

Regarding possible limitations of using indoor radon data, it is possible that temporal variations of indoor radon and seasonal adjustments for representing annual average radon concentrations may also generate errors that are difficult to quantify. It is also difficult to extract all factors that may affect indoor radon concentration. Indoor radon maps may therefore be biased by the sampling method and by dwellings where radon prevention measures were installed but not reported in the survey. Furthermore, radon maps based on indoor radon measurements require a high number of individual measurements, which are normally taken over several years, meaning indoor radon data may be affected by seasonal and year-to-year variations.

Table 6. Indoor radon concentration summary statistics for each GRP classification

GRP	Indoor radon		Sampled dwellings			Binomial distribution		
	GM	GSD	≤R.L.	>R.L.	Total	Prob.	LCI	UCI
L	47.49	2.36	2,186	142	2,328	6.10	5.16	7.15
M–L	57.90	2.48	6,603	714	7,317	9.76	9.09	10.46
M–H	70.61	2.65	4,549	759	5,308	14.30	13.37	15.27
H	98.65	3.01	1,349	486	1,835	26.49	24.48	28.57
Total	63.58	2.63	14,687	2,101	16,788	12.51	12.02	13.02

Reference level (R.L.) = 200 Bq m^{-3}; probabilities (Prob.) in %; LCI and UCI are the 95% lower and upper confidence limit, respectively. *L: Low, M–L: Moderate–Low, M–H: Moderate–High, H: High; GM, geometric mean; GSD, geometric standard deviation in Bq m^{-3}; GRP, geogenic radon potential.*

It is anticipated that the average indoor radon concentration, and so the radon risk, in a given area may decrease with the implementation of radon action plans. Given that radon classification for a specific area may then change over time, it may not be best practice to merge radon surveys over different years, especially when metadata on remediation are not available. In this regard, an area classified as High risk may a few years later effectively be classified with a lower radon risk in a subsequent survey. We have attempted to remove this unintended bias in indoor radon datasets by only using the first measurements from a given property. However, we cannot exclude the possibility that we have inadvertently used indoor radon measurements from homes that have been remediated or have a radon barrier. In the case of this study, the indoor radon measurements have been used to validate our model, rather than train it. The fact that we see a good agreement between GRP categories and the GM of indoor radon for these designated areas suggests that the model performs well, despite the possibility that we may have inadvertently included some remediated properties in the model validation exercise.

The inherent spatial variability of soil gas radon concentrations over small distances does not allow a precise relationship between soil gas Rn and airborne Ra to be computed. However, a broad correlation between soil gas Rn and airborne Ra concentrations can be discerned. The predicted capacity of the resulting map may be improved by including both the influence of water saturation on soil permeability (i.e. reducing it) (51) and the possible increase of the emanation factor (ε) due to water saturation (i.e. increasing it) (46, 47). It would be also beneficial for the model to differentiate between soil types (i.e. ε, ρ, and n). Finally, an optimization of the RP thresholds (Table 2) may also be applied for taking into account the specific characteristics of the building stock and living styles of a country in the risk assessment.

Acknowledgments

Many thanks to Luka Vucinic, Eamonn Burke, and Stephen Wolfe (Trinity College, Dublin) and Richard Turley (Geological Survey, Ireland) for their assistance in the field. The sole responsibility of this publication lies with the authors. The GSI is not responsible for any use that may be made of the information contained therein. Data used in this project were collated as part of the Tellus projects (http://www.tellus.ie) and also by the Environmental Protection Agency of Ireland.

Conflict of interest and funding

The authors declare no conflict of interest.This work was financed by the Geological Survey, Ireland (GSI Research Programme Short Call 2017; Ref. Number: 2017-SC-008). The Environmental Protection Agency of Ireland was also partly financed the present study for purchasing the required instrumentation.

References

1. WHO. WHO handbook on indoor radon: a public health perspective. Zeeb H, Shannoun F, eds. Vol. 67. France: World Health Organization; 2009.
2. Gaskin J, Coyle D, Whyte J, Krewksi D. Global estimate of lung cancer mortality attributable to residential radon. Environ Health Perspect 2018 May 31; 126(5): 1–8. doi: 10.1289/EHP2503
3. Darby S, Hill D, Auvinen A, Barros-Dios JM, Baysson H, Bochicchio F, et al. Radon in homes and risk of lung cancer: collaborative analysis of individual data from 13 European case-control studies. BMJ 2005 Jan 29; 330(7485): 223. doi: 10.1136/bmj.38308.477650.63
4. Fuente M, Rábago D, Goggins J, Fuente I, Sainz C, Foley M. Radon mitigation by soil depressurisation case study: radon concentration and pressure field extension monitoring in a pilot house in Spain. Sci Total Environ 2019; 695: 133746. doi: 10.1016/j.scitotenv.2019.133746
5. NRCS (National Radon Control Strategy). Minister for the Environment (Ireland); 2014.
6. Miles J, Appleton J, Rees D. Indicative atlas of radon in England and Wales (Report HPA-RPD-033). Health Protection Agency and British Geological Survey; 2007, pp. 1–29.
7. EURATOM. Council directive 2013/59/EURATOM of 5 December. Offic J Eur Union (Nº L13) 2013.
8. Bossew P. Radon priority areas – definition, estimation and uncertainty. Nucl Technol Radiat Prot 2018; 33(3): 286–92. doi: 10.2298/NTRP180515011B
9. Bochicchio F, Venoso G, Antignani S, Carpentieri C. Radon reference levels and priority areas considering optimisation and avertable lung cancers. Radiat Prot Dosimetry 2017; 177(1–2): 87–90. doi: 10.1093/rpd/ncx130
10. EPA. National radon control strategy, phase two: 2019–2024, report of the National Radon Control Strategy Coordination Group. 2019. Available from: http://www.epa.ie/pubs/reports/radiation/nrcsphase2.html
11. Elío J, Crowley Q, Scanlon R, Hodgson J, Zgaga L. Estimation of residential radon exposure and definition of Radon Priority Areas based on expected lung cancer incidence. Environ Int. 2018; 114: 69–76. doi: 10.1016/j.envint.2018.02.025
12. Elío J, Crowley Q, Scanlon R, Hodgson J, Long S. Logistic regression model for detecting radon prone areas in Ireland. Sci Total Environ 2017 Dec; 599–600: 1317–29. doi: 10.1016/j.scitotenv.2017.05.071
13. Minda M, Tóth G, Horváth I, Barnet I, Hámori K, Tóth E. Indoor radon mapping and its relation to geology in Hungary. Environ Geol 2009; 57(3): 601–9. doi: 10.1007/s00254-008-1329-6
14. Fennell SG, Mackin GM, Madden JS, Mcgarry AT, Duffy JT, Colgan PA, et al. Radon in dwellings the Irish National Radon Survey (Report RPII-02/1). Radiological Protection Institute of Dublin, Ireland; 2002, 41 p.
15. Friedmann H. Final results of the Austrian Radon Project. Health Phys 2005 Oct; 89(4): 339–48. doi: 10.1097/01.HP.0000167228.18113.27
16. Friedmann H, Gröller J. An approach to improve the Austrian Radon Potential Map by Bayesian statistics. J Environ Radioact 2010 Oct; 101(10): 804–8. doi: 10.1016/j.jenvrad.2009.11.008

17. Watson RJ, Smethurst MA, Ganerød GV, Finne I, Rudjord AL. The use of mapped geology as a predictor of radon potential in Norway. J Environ Radioact 2017 Jan; 166: 341–54. doi: 10.1016/j.jenvrad.2016.05.031
18. Elío J, Cinelli G, Bossew P, Gutiérrez-Villanueva JL, Tollefsen T, De Cort M, et al. The first version of the Pan-European Indoor Radon Map. Nat. Hazards Earth Syst. Sci., 19, 2019; 2451–2464. doi: 10.5194/nhess-19-2451-2019
19. Dubois G, Bossew P, Tollefsen T, De Cort M. First steps towards a European atlas of natural radiation: status of the European indoor radon map. J Environ Radioact 2010; 101(10): 786–98. doi: 10.1016/j.jenvrad.2010.03.007
20. Bossew P. Mapping the geogenic radon potential and estimation of radon prone areas in Germany. Radiat Emerg Med 2015; 4(2): 13–20.
21. Bossew P. Determination of radon prone areas by optimized binary classification. J Environ Radioact 2014 Mar; 129: 121–32. doi: 10.1016/j.jenvrad.2013.12.015
22. Alharbi WR. Measurement of radon concentrations in soil and the extent of their impact on the environment from Al-Qassim, Saudi Arabia. Nat Sci 2013; 05(01): 93–8. doi: 10.4236/ns.2013.51015
23. Gunby JA, Darby SC, Miles JCH, Green BMR, Cox DR. Factors affecting indoor radon concentrations in the United Kingdom. Health Phys 1993; 64(1): 2–12. doi: 10.1097/00004032-199301000-00001
24. Borgoni R, De Francesco D, De Bartolo D, Tzavidis N. Hierarchical modeling of indoor radon concentration: how much do geology and building factors matter? J Environ Radioact 2014; 138: 227–37. doi: 10.1016/j.jenvrad.2014.08.022
25. Neznal M, Neznal M, Matolín M, Barnet I, Mikšová J. New method for assessing the radon risk of building sites. Czech Geol Surv Spec Pap; 2004. p. 47.
26. Elío J, Crowley Q, Scanlon R, Hodgson J, Long S. Rapid radon potential classification using soil-gas radon measurements in the Cooley Peninsula, County Louth, Ireland. Environ Earth Sci 2019; 78(12): 359. doi: 10.1007/s12665-019-8339-4
27. SGL. Technical report: fixed-wing high-resolution aeromagnetic, gamma-ray spectrometric and frequency-domain electromagnetic survey. Ottawa, Canada: Tellus A7 Block, Republic of Ireland 2019 for Geological Survey, Ireland; 2019.
28. Adepelumi AA, Ajayi TR, Ako BD, Ojo AO. Radon soil-gas as a geological mapping tool: case study from basement complex of Nigeria. Environ Geol 2005; 48(6): 762–70. doi: 10.1007/s00254-005-0016-0
29. Cothern R, Smith J. Environmental radon. Cothern CR, Smith EJ, eds. New York: Plenum Press; 1987, 363 p.
30. Guerra M, Lombardi S. Soil-gas method for tracing neotectonic faults in clay basins: the Pisticci field (Southern Italy). Tectonophysics 2001; 339(3–4): 511–22. doi: 10.1016/S0040-1951(01)00072-5
31. Schubert M, Freyer K, Treutler HC, Weiß H. Using the soil gas radon as an indicator for ground contamination by non-aqueous phase-liquids. J Soils Sediments 2001; 1(4): 217–22. doi: 10.1007/BF02987728
32. Elío J, Ortega MF, Nisi B, Mazadiego LF, Vaselli O, Caballero J, et al. CO2 and Rn degassing from the natural analog of Campo de Calatrava (Spain): implications for monitoring of CO2 storage sites. Int J Greenh Gas Control 2015; 32: 1–14. doi: 10.1016/j.ijggc.2014.10.014
33. Schubert M, Schmidt A, Muller K, Weiss H. Using radon-222 as indicator for the evaluation of the efficiency of groundwater remediation by in situ air sparging. J Environ Radioact 2011; 102(2): 193–9. doi: 10.1016/j.jenvrad.2010.11.012
34. IAEA. Guidelines for radioelement mapping using gamma ray spectrometry data, IAEA-TECDOC-1363. International Atomic Energy Agency, Vienna, Austria; 2003.
35. Yu C, Loureiro C, Cheng JJ, Jones LG, Wang YY, Chia YP, et al. Data collection handbook to support modeling impacts of radioactive materialsin soil. Argonne, IL: Environmental Assessment and Information Sciences Division, ArgonneNational Laboratory; 1993.
36. GSI. Groundwater Resources (Aquifers). Available from: https://www.gsi.ie/en-ie/data-and-maps/Pages/Groundwater.aspx#Aquifers [cited 16 April 2020].
37. Roberson S, Pellicer X. An all Ireland quaternary map. In: Geophysical research Abstracts. Vienna, Austria: 19th EGU General Assembly, EGU2017, proceedings from the conference held 23–28 April, Vienna, Austria; 2017. p.13365
38. GSI. Quaternary sediments. Available from: https://dcenr.maps.arcgis.com/home/item.html?id=1bbf22e9391c484db4b84e-4150313bae [cited 16 April 2020].
39. Appleton JD, Daraktchieva Z, Young ME. Geological controls on radon potential in Northern Ireland. Proc Geol Assoc 2015 Jun; 126(3): 328–45. doi: 10.1016/j.pgeola.2014.07.001
40. Appleton JD, Miles JCH, Young M. Comparison of Northern Ireland radon maps based on indoor radon measurements and geology with maps derived by predictive modelling of airborne radiometric and ground permeability data. Sci Total Environ 2011 Mar 15; 409(8): 1572–83. doi: 10.1016/j.scitotenv.2011.01.023
41. GSI. All Ireland Quaternary Map 500k (scale 1:500.000). Available from: https://secure.dccae.gov.ie/GSI_DOWNLOAD/Quaternary/Data/Quaternary_500k_All_Ireland_Map.pdf [cited 18 January 2020].
42. Neznal M, Neznal M. Analysis of problems and failures in the measurement of soil-gas radon concentration. Radiat Prot Dosimetry 2014 Jul 1; 160(1–3): 214–16. doi: 10.1093/rpd/ncu088
43. Daraktchieva Z, Appleton JD, Rees DM, Adlam KAM, Myers AH, Hodgson SA, et al. Radon in Northern Ireland: indicative atlas. Public Health England (Report PHE-CRCE-017). London. 2015.
44. Hodgson J, Carey S, Scanlon R. Developing a new National Radon Risk Map. Geological Survey, Ireland; 2014.
45. HSE-RPII. Radon gas in Ireland joint position statement by the Radiological Protection Institute of Ireland and the Health Service Executive (HSE) and the Radiological Protection Institute of Ireland (RPII). Radon gas in Ireland joint position statement. Dublin, Ireland; 2010.
46. Zhuo W, Iida T, Furukawa M. Modeling radon flux density from the earth's surface. J Nucl Sci Technol 2006; 43(4): 479–82. doi: 10.3327/jnst.43.479
47. Bossew P. The radon emanation power of building materials, soils and rocks. Appl Radiat Isot 2003; 59(5–6): 389–92. doi: 10.1016/j.apradiso.2003.07.001
48. Nasuti A, Roberts D, Dumais M-A, Ofstad F, Hyvönen E, Stampolidis A, et al. New high-resolution aeromagnetic and radiometric surveys in Finnmark and North Troms: linking anomaly patterns to bedrock geology and structure. Nor J Geol 2016; 95(3): 217–43. doi: 10.17850/njg95-3-10
49. Minty B, Franklin R, Milligan P, Richardson M, Wilford J. The radiometric map of Australia. Explor Geophys 2009; 40(4): 325–33. doi: 10.1071/EG09025
50. Siemon B, Costabe S, Voß W, Meyer U, Deus N, Elbracht J, et al. Airborne and ground geophysical mapping of coastal clays in

Eastern Friesland, Germany. Geophysics 2015; 80(3): WB21–34. doi: 10.1190/geo2014-0102.1

51. Benavente D, Valdés-Abellán J, Pla C, Sanz-Rubio E. Estimation of soil gas permeability for assessing radon risk using Rosetta pedotransfer function based on soil texture and water content. J Environ Radioact 2019; 208–209: 105992. doi: 10.1016/j.jenvrad.2019.105992

***Elío J.**
Centre for the Environment
Trinity College
Dublin 2
Ireland
Email: javiereliomedina@gmail.com

Citation: Journal of the European Radon Association 2020, **1**: 4358 http://dx.doi.org/10.35815/radon.v1.4358